Cryo-EM structure of alpha-synuclein fibrils

Ricardo Guerrero-Ferreira[1], Nicholas M.I. Taylor[1]†, Daniel Mona[2], Philippe Ringler[1], Matthias E. Lauer[3], Roland Riek[4], Markus Britschgi[2], and Henning Stahlberg[1,]*.

[1] Center for Cellular Imaging and NanoAnalytics (C-CINA), Biozentrum, University of Basel, Mattenstrasse 26, 4058 Basel, Switzerland.

[2] Roche Pharma Research and Early Development, Neuroscience, Ophthalmology and Rare Diseases Discovery and Translational Area/Neuroscience Discovery, Roche Innovation Center Basel, Basel, Switzerland.

[3] Roche Pharma Research and Early Development, Chemical Biology, Roche Innovation Center Basel, Basel, Switzerland.

[4] Laboratory of Physical Chemistry, ETH Zürich, 8093 Zürich, Switzerland.

*Correspondence to: Henning Stahlberg (henning.stahlberg@unibas.ch).

†Current Address: Structural Biology of Molecular Machines Group, Protein Structure & Function Programme, Novo Nordisk Foundation Center for Protein Research, Faculty of Health and Medical Sciences, University of Copenhagen, Blegdamsvej 3B, Copenhagen 2200, Denmark.

Abstract

Parkinson's disease is a progressive neuropathological disorder that belongs to the class of synucleopathies, in which the protein alpha-synuclein is found at abnormally high concentrations in affected neurons. Its hallmark are intracellular inclusions called Lewy bodies and Lewy neurites. We here report the structure of cytotoxic alpha-synuclein fibrils (residues 1-121), determined by cryo-electron microscopy structure at a resolution of 3.4Å. Two protofilaments form a polar fibril composed of staggered β-strands. The backbone of residues 38 to 95, including the fibril core and the non-amyloid component region, are well resolved in the EM map. Residues 50-57, containing three of the mutation sites associated with familial synucleinopathies, form the interface between the two protofilaments and contribute to fibril stability. A hydrophobic cleft at one end of the fibril may have implications for fibril elongation, and invites for the design of molecules for diagnosis and treatment of synucleinopathies.

Impact Statement

The alpha-synuclein fibril structure reported here buries residues 50-57 at the interface between its two protofilaments, suggesting that familial Parkinson's disease associated mutations in these residues lead to a structure not compatible with the one presented here.

Introduction

Parkinson's disease (PD) is a neurodegenerative disorder characterized by the presence of Lewy bodies (LB) and Lewy neurites (LN). Spillantini et al. (1997) identified fibrils formed by the presynaptic protein alpha-synuclein (α-Syn, 140 residues, ~14 kD) as the main component of these human brain inclusions (Spillantini et al., 1998; Spillantini et al., 1997).

Certain α-Syn fibril forms can seed LB-like and LN-like inclusions in cell culture and intra-neuronal aggregation of mouse α-Syn *in vivo* (Luk et al., 2009; Thakur et al., 2017; Volpicelli-Daley et al., 2014). In addition, abnormal α-Syn produces neuronal cell inclusions and axonal spheroids, as well as oligodendrocytic aggregates, known as glial cytoplasmic inclusions, found abundantly in Multiple System Atrophy (MSA) (Arima et al., 1998; Tu et al., 1998), which makes α-Syn fibrils an important target for the development of diagnostic tools and therapeutic strategies for PD and related synucleinopathies.

Despite α-Syn fibrils, other forms of α-Syn might also be involved in neurodegeneration, such as an oligomeric α-Syn intermediate (Danzer et al., 2007; Lashuel et al., 2002; Outeiro et al., 2008; Vicente Miranda et al., 2017; Villar-Pique et al., 2016; Winner et al., 2011), or the process of fibril aggregation itself (Oueslati et al., 2010; Reynolds et al., 2017; Taschenberger et al., 2012). Fibrils of α-Syn show significant fibril strain polymorphism (Peelaerts et al., 2015).

Several factors point to α-Syn as an important player in the onset of PD: (i) six known point mutations in the α-Syn gene (SNCA) are associated with familial forms of synucleinopathies: A30P (Kruger et al., 1998), E46K (Zarranz et al., 2004), H50Q (Appel-Cresswell et al., 2013), G51D (Lesage et al., 2013), A53E (Pasanen et al., 2014), and A53T (Polymeropoulos et al., 1997); (ii) animal models suggest a role of α-Syn in the etiology of PD, Dementia with Lewy Bodies (DLB), and MSA (Feany and Bender, 2000; Hashimoto et al., 2003; Periquet et al., 2007; Tyson et al., 2017); (iii) individuals with duplications or triplications of the α-Syn gene exhibit overexpression of α-Syn and develop PD (Ibanez et al., 2004; Singleton et al., 2003).

Two related proteins, β-synuclein (β-Syn) and γ-synuclein (γ-Syn), with sequence homology to α-Syn, have been described (Clayton and George, 1998; Jakes et al., 1994; Stefanis, 2012). β-Syn and α-Syn share the greatest aminoacid sequence homology, with β-Syn lacking 12 amino acids (residues 71 to 82) within the non-amyloid component region (NAC; residues 61-95 in α-Syn) (Giasson et al., 2001; Ueda et al., 1993). In synucleins, regions with the highest homologies are located in the structurally heterogeneous, amino-terminal half (residues 10-84 in α-Syn) composed of 5 to 6 imperfect repeats with the consensus sequence KTKEGV (Der-Sarkissian et al., 2003). In contrast, the carboxyl terminus is highly negatively charged and unstructured (Chen et al., 2007; Vilar et al., 2008).

A number of post-translational modifications have been described for α-Syn including phosphorylation (Anderson et al., 2006; Fujiwara et al., 2002; Paleologou et al., 2010), acetylation (Iyer et al., 2016; Maltsev et al., 2012), ubiquitination (Hasegawa et al., 2002), and C-terminal truncation (Anderson et al., 2006; Crowther et al., 1998). C-terminal truncation of α-Syn occurs normally *in vivo*, under physiological conditions and it has been shown to promote fibrillization (Crowther et al., 1998; Li et al., 2005; Liu et al., 2005; Wang et al., 2016). In turn, truncated forms of α-Syn play a role in inducing Lewy body formation (Dufty et al., 2007; Li et al., 2005; Prasad et al., 2012), suggesting that truncation by proteolysis may be important in the pathological process.

In vivo studies investigating α-Syn aggregation demonstrated that activation of the inflammasome and more specifically caspase-1, the enzymatic component of the

inflammasome, leads to the production of an α-Syn fragment truncated at aspartic acid 121 (D121) (Wang et al., 2016). This C-terminally-truncated α-Syn form (α-Syn(1-121)) aggregates more rapidly than full-length α-Syn (including disease-associated mutants), and its production is associated with cell toxicity. Furthermore, the use of VX-765, a pro-drug that produces a specific inhibitor of caspase-1 *in vivo* (Wannamaker et al., 2007), improved survival of a neuronal cell model of PD (Wang et al., 2016), and reduced neurodegeneration in a transgenic mouse model of MSA (Bassil et al., 2016), suggesting an important role of α-Syn(1-121) for cellular toxicity in both, cell cultures as well as a mouse mode.

To this date, high resolution structures of α-Syn fibrils are limited to the results of a micro-electron diffraction (microED) study of two small segments of the protein (Rodriguez et al., 2015) and a solid-state NMR structure obtained from ~5 nm diameter, single protofilaments (Tuttle et al., 2016), in addition to solid state NMR studies at the secondary structure level (Bousset et al., 2013; Kim et al., 2009; Vilar et al., 2008), and X-ray diffraction studies of shorter segments of α-Syn (Li et al., 2014), or α-Syn bound to other molecules (De Genst et al., 2010; Gruschus et al., 2013; Rao et al., 2010; Ulmer et al., 2005; Xie et al., 2010; Yagi-Utsumi et al., 2015; Zhao et al., 2011).

Here, we report the atomic structure of α-Syn(1-121) fibrils determined by cryo-electron microscopy (cryo-EM). The structure allows conclusions about the organization of α-Syn fibrils at near-atomic resolution and suggest mechanisms for fibril formation and growth, and allows conclusions on fibril stability.

Results and Discussion

The 3D structure of α-Syn amyloid fibrils

Several preparations of recombinant human α-Syn fibril were screened by negative stain transmission electron microscopy (TEM; Figure 1 – figure supplement 1). These included fibrils formed by full length α-Syn (Figure 1A), α-Syn phosphorylated at serine 129, N-terminally acetylated, and C-terminal truncated α-Syn comprised of residues 1-119 (α-Syn(1-119)), 1-121 (α-Syn(1-121)), or 1-122 (α-Syn(1-122)).

The diameters of the α-Syn fibrils produced varied from 5 nm to approximately 10 nm when studied by negative stain TEM. The fibrils formed by α-Syn(1-121) were straight, between 20 and 500 nm long and the only ones of consistent diameters of 10 nm (Figure 1B, Figure 1 – figure supplement 1E). This fibrillar form α-Syn(1-121) has been described as an aggregation-prone species resulting from α-Syn truncation by caspase-1 (Wang et al., 2016). The recombinantly produced α-Syn(1-121) used here showed a similarly aggressive aggregation profile.

Preparations of α-Syn(1-121) fibrils were quick-frozen in the holes of fenestrated carbon coated cryo-electron microscopy (cryo-EM) grids, and imaged with a Titan Krios 300kV cryo-EM instrument, equipped with a Quantum-LS energy filter and a K2 Summit direct electron detector. Helical image processing of recorded cryo-EM movies produced a 3D reconstruction of the α-Syn(1-121) fibril at an overall resolution of 3.4 Å (Figure 1C and D, Figure 1 – figure supplement 2, Figure 2, and Video 1).

Our 3D map shows that fibrils are formed by two protofilaments, each of 5 nm in diameter (Figure 1). These lack C2 symmetry, but are related by an approximate 2_1 screw symmetry, akin to the symmetry exhibited by the paired helical filaments of tau (Fitzpatrick et al., 2017) and by amyloid-ß(1-42) filaments (Gremer et al., 2017). α-Syn(1-121) fibrils are therefore polar, meaning that both protofibrils are aligned into the same direction. The position of a given ß-sheet in a protofilament is produced by the rotation of -179.5° of one sheet around its axis (helical twist), followed by a vertical translation of 2.45 Å (helical rise). This ß-sheet arrangement results in a spacing of 4.9 Å between α-Syn subunits in successive rungs of a single protofilament (Figure 1C and D). The quality of the EM map allowed an atomic model of the region between residues L38 and V95 to be built.

Each α-Syn(1-121) molecule comprises eight in-register parallel β-strands (*i.e.*, residues 42-46 (β1), 48-49 (β2), 52–57 (β3), 59–66 (β4), 69-72 (β5), 77–82 (β6), 89-92 (β7), and 94-(~102) (β8)), which are interrupted by glycine residues (*i.e.*, G41 before β1, G47 between β1 and β2, G51 between β2 and β3, G67 and G68 between β4 and β5, G73 between β5 and β6, G84 and G86 between β6 and β7, and G93 between β7 and β8) or an arch (*i.e.*, E57-K58 between β3 and β4) (Figure 1A, F, and G). The β-strands β2-β7 wind around a hydrophobic intra-molecular core composed of only alanine and valine residues and one isoleucine (*i.e.*, V48, V49, V52, A53, V55, V63, A69, V70, V71, V74, A76, V77, A78, I88, A89, A90, A91). Considering that these hydrophobic clusters are maintained along the fibril, they are likely to contribute to the stability of the protofilament. The hydrophobic core is surrounded by two hydrophilic regions (*i.e.* (i): Q79, T81, and (ii): T72, T75, T54, T59, and E61) both still within the core of the structure (Figure 3). While most of these side chains form so-called side chain hydrogen bond ladders (Nelson et al., 2005; Riek, 2017), the second hydrophilic region comprising four threonine residues and a negatively charged glutamic acid side chain surrounds a tunnel filled with some ordered molecules of unknown nature, as evidenced by an additional density (Figure 1- figure supplement 3D). The less well defined β1 and β8 strands are attached to the core, while the first 37 N-terminal residues and the last ~20 C-

terminal residues of α-Syn(1-121) are not visible in the 3D reconstruction (Figure 1E and Figure 1 – figure supplement 2A), indicating a disordered structure in line with quenched hydrogen/deuterium exchange – solution-state NMR (H/D exchange NMR) and limited proteolysis (Vilar et al., 2008), which showed these terminal segments to be unprotected in nature. Together with our results, this suggests that approximately 40 residues of both the N- and C-terminal ends of full-length human α-Syn are flexible, and surround the structured core of the fibril with a dense mesh of disordered tails, similar to the 'fuzzy coat' recently described in the cryo-EM Tau structure (Fitzpatrick et al., 2017).

Two β-sheets (one from each protofilament) interact at the fibril core via a hydrophobic steric zipper-geometry comprised of β-strand β3 (*i.e.*, residues G51-A56). As a consequence, two α-Syn molecules per fibril layer are stacked along the fibril axis (Figure 2B and C). The side chains of residues A53 and V55 form the inter-molecular surface contributing to the interface between the two protofilaments, which is further stabilized by a surface-exposed salt bridge between E57 and H50 that might be sensitive to pH, as an unprotected histidine has a pK of ~6.2 (Figure 1 – figure supplement 3H). The same structure with a steric zipper topology was found in micro-crystals of the peptide comprising residues G47-A56 (Rodriguez et al., 2015). Interestingly, the β-strand β6 that is sandwiched between β-strands β2/β3 and β7 is also aligned with a neighboring molecule but shifted by one monomer along the fibril axis, as shown in Figure 1G and Figure 2 – figure supplement 1. Thus, hetero and homo steric zippers are both present in the 3D structure. Of these, the homo steric zipper at the inter-molecular interface has an extensive and well-packed β-strand interface, forming a very densely packed fibril. This stacking generates an asymmetric fibril with two distinct ends. Furthermore, the hydrophobic core of the fibril is composed of β-strands that interact with each other in a half-stacked zipper topology, contrasting with the hydrophilic core comprised of β-strands β4 and β5, which are non-stacked (Figure 1G and Figure 2 – figure supplement 1). The latter confirms previous results from site-directed spin labeling experiments, which show that the region including residues 62-67 at the beginning of the NAC region, has a pronounced lack of stacking interactions (Chen et al., 2007).

The outer surface of the ordered region of the fibrils is mostly hydrophilic, with a few exceptions (*i.e.*, L38, V40, V82, A85, A90, F94, V95) (Figure 3A). The side chain of V66 should probably not be classified as surface exposed because of its interaction with β-strand β8 (Figure 1 – figure supplement 2A). If we ignore the influence of the non-polar alanine residues due to the small size of their side chains, the surface of the fibrils has two highly hydrophobic regions formed by residues L38 and V40, and by residues F94 and V95. Other interesting properties of the surface are the salt bridge formed by the side chains of E46 and K80 (Figure 1 – figure supplement 3G) and the rather highly positive clustering of K43, K45, K58, H50 that requests the binding of a counter-ion, as it is supported by an observed density (Figure 1 – figure supplement 3C).

The familial PD mutations in the context of the 3D fibril structure

Six familial mutations in α-Syn are known to be associated with PD and other synucleinopathies (*i.e.*, A30P, E46K, H50Q, G51D, A53E, and A53T). Of these, all but A30P are located in the heart of the core of the fibril structure presented here (Figure 1A and E). E46 forms a salt bridge with K80 (Figure 1 – figure supplement 3G). The mutation of the glutamic acid E46 to a positively charged lysine in an E46K mutant would thus induce a charge repulsion between β-strands β1 and β6, likely destabilizing this α-Syn fibril structure (Tuttle et al., 2016). The familial PD/DLB-causing mutation E46K was found to enhance phosphorylation in mice (Mbefo et al., 2015), and its toxic effect was increased by the triple-K mutation (E35K, E46K, E61K) in neuronal cells (Dettmer et al., 2017).

Previous high-resolution structures of α-Syn only included small peptides or single protofilaments (Rodriguez et al., 2015; Tuttle et al., 2016). Our 3D map suggests structural contributions of some familial mutations to fibril stability, since H50, G51 and A53 are all involved in the inter-molecular contact between the two β-sheets from adjacent protofilaments at the core of the here studied α-Syn(1-121) fibrils. Mutation of the positively charged histidine 50 into a polar, uncharged glutamine in the H50Q mutant would likely interfere with the salt bridge established between residues E57 and H50 (Figure 1 – figure supplement 3H). Adding to the absent side-chain of glycine 51 a negatively charged aspartic acid in mutant G51D, or transforming the small side-chain of alanine A53 into a larger threonine in mutant A53T, would likely disrupt the steric zipper interaction between the two protofibrils, whereby the A53T mutation would in addition change the highly hydrophobic surface at the zipper to partly hydrophilic one. In our α-Syn(1-121) fibril structure, A53 is part of a hydrophobic pocket that defines the interaction of protofilaments and likely contributes to fibril stability as the hydrophobic interactions exist along the fibril axis. Mutations at the core of this α-Syn fibril would compromise the formation of the structure presented here. This suggests that a different fibril structure (*i.e.*, fibril strain) could be formed from α-Syn containing the above discussed familial PD mutations.

Several features of our structure, such as non-functional hydrophobic surface patches (Figure 3), a hydrophilic tunnel (Figure 1 – figure supplement 3D), and a positively charged side chain arrangement like the one comprised of residues K43, K45, K58, H50 (Figure 1 – figure supplement 3C) are not found in functional amyloid structures such as that of HET-s (Wasmer et al., 2008). However, similar structural characteristics have been previously observed for pathological Tau filaments obtained from Alzheimer's disease brains where (i): lysine and tyrosine residues play a similarly stabilizing role in the interface region of two protofilaments of the straight filaments (SF), and (ii): the area in the center of the protofilaments is dominated by hydrophilic residues (Fitzpatrick et al., 2017). It is plausible that these structural features might arise because folding to form the amyloid fibril structure is dictated by the need to bury the maximum number of hydrophobic side-chains as efficiently as possible, as is also the case for the Aβ(1-42) amyloid fibrils (Gremer et al., 2017).

The artificial, highly toxic, but not synucleinopathy-related mutant E57K (Winner et al., 2011) is interesting to mention in the context of the 3D structure presented, because E57 is also at the inter-molecular interface (Figure 2). The presence of a positive lysine side chain at this position in the E57K mutant would significantly interfere with the formation of the interface and even the amyloid fibril (Winner et al., 2011). Indeed, this mutant was designed in a successful structure-based attempt to interfere with amyloid fibril formation (at least under some conditions) (Winner et al., 2011). Furthermore, both in a lentivirus-rat system as well as in a transgenic mouse model, the E57K mutant formed a significant amount of oligomers and was highly toxic, resulting in a large decay of TH-sensitive neurons in the *Substantia nigra* of rats and a motor phenotype reminiscent of PD in mice (Winner et al., 2011). Thus, the artificial mutant E57K can be regarded as a "familial PD-like" mutation both from the *in vivo* and from the structure/mechanism-based point of view.

Comparison with earlier structural data

Full-length α-Syn subunits in a fibril studied by NMR ((Tuttle et al., 2016), PDB 2N0A) were found to in a roughly similar secondary structure arrangement as in the here reported structure of α-Syn(1-121) (Figure 4A), even though the primary structure and the side-chain interactions of our here reported structure are very different from the NMR structure. Most importantly, the fibrils used for the NMR study were only approximately 5 nm wide, which

corresponds to the diameter of a single protofilament. The larger diameter of our fibrils, 10 nm, results from the interaction between two protofilaments, which allowed us to hypothesize on the nature of α-Syn(1-121) protofilament interactions. Fibrils of 5 to 10 nm in diameter were found in *substantia nigra* samples from the brain of PD patients, (Crowther et al., 2000), cingulate cortex of patients with DLB (Spillantini et al., 1998), cerebral cortex of PD patients (Kosaka et al., 1976), and in-vitro aggregated samples (Bousset et al., 2013). Crowther et al. (2000) had already suggested that the 10 nm filaments are the result of the interaction between 5 nm protofilaments.

An important difference between our here reported structure and the NMR structure reported by (Tuttle et al., 2016) is the orientation of residue A53. The mutation A53T is associated with early onset PD. In our structure, residue A53 faces the interface between the two protofibrils and thereby likely contributes to fibril stability. In contrast, Tuttle et al. (2016) reported in their NMR structure A53 to point towards the hydrophobic core of the one observed individual protofilament, which may explain the lack of 10 nm fibrils in their sample. However, it is also noted here that the NMR study by Tuttle et al. (2016) showed a significant disagreement among the ten lowest-energy NMR structures for residues 51-67 (Figure 3d in (Tuttle et al., 2016)), indicating a lower confidence for those residues in the NMR structure. Our here reported cryo-EM map has the side-chains for those residues pointing into the opposite direction as reported in the Tuttle et al. (2016) structure.

Our structure includes a serine residue at position 87 (Figure 1 – figure supplement 3E), which is one of the several phosphorylation sites in α-Syn, in addition to Y125, S129, Y133 and Y135 (Oueslati et al., 2012; Paleologou et al., 2010). S87 is the only phosphorylation site located within the NAC region. The previous solid-state NMR structure of α-Syn placed the side chain of this residue towards the inside of the protofilament core, leading to the assumption that phosphorylation of S87 might be the only modification occurring at a region not accessible in the fibrillar state. However, in our cryo-EM structure, S87 faces the outside of the fibril and hence remains accessible for disease-associated modification in α-Syn fibrils.

We also observed the arrangement of G47 and A78 described by Tuttle *et al.* (2016), which was proposed to favor the interaction between residues E46 and K80 and allow them to form a stable salt bridge between two consecutive α-Syn monomers (Figure 1 – figure supplement 3G). The conservation of the geometry adopted by these residues confirms their role in facilitating backbone-backbone interactions. In addition, our structure also confirms that residues A69 and G93 (and likely G68) help to stabilize the distal loop in a protofilament (Figure 1 – figure supplement 3F).

A microED structure obtained from crystals produced from a 10-residue peptide simulating the core of α-Syn fibrils (PreNAC, from 47 to 56; Figure 4B) and including a threonine instead of an alanine at position 53 (*i.e.*, A53T), also proposed that residue 53 forms the hydrophobic core within a protofilament (Rodriguez et al., 2015). In addition, the microED model suggested that the interaction between adjacent protofilaments would occur through residues 68 to 78 (referred to as NACore) (Rodriguez et al., 2015). However, their short peptides did not include most residues responsible for the α-Syn monomer topology that we observed. Instead, our cryo-EM structure reveals that the PreNAC is responsible for the interaction between protofilaments, and places the NACore at the very center (*i.e.*, the core) of a single protofilament.

Possible mechanism of fibril elongation

Our 3D structure allows us to hypothesize a mechanism for fibril elongation (fibril growth). Because two different stacking modes are present (*i.e.*, the half-stack at the intermolecular

interface and the stacking of β-strand β6), the two ends of the fibrils are distinct, suggesting an end-dependent growth of the fibrils, as documented and also suggested for other amyloids (Luhrs et al., 2005). One end of the fibril includes a hydrophobic cleft formed between β-strands β2/ β3 on one side and β7 on the other side (residues V49, V52, A88, I89), providing a hydrophobic entry point for the next incoming molecule, with the matching segment consisting of 5 hydrophobic residues (V74-V82, Figure 5). This suggests that the initial binding event of fibril elongation might be a hydrophobic interaction involving residues V74-V82. This peptide segment is the central part of the NAC region and strong experimental evidence suggests that it is critical for fibril formation (Giasson et al., 2001). In addition, it has been shown that β-synuclein, which lacks residues V74 to V82, is incapable of forming fibrils (Giasson et al., 2001).

It is intriguing to speculate that a small molecule binding into this hydrophobic cleft could be a potent fibril elongation inhibitor or tracer, with the potential to be applied in PD and other synucleinopathies. Finally, the inter-molecular stacking may also play a role in fibril elongation, since the zipper interaction is of hydrophobic nature. Furthermore, it is likely that fibril growth alternates between the two protofilament structures at the level of monomer addition. Failure thereof may result in the growth of a single protofilament with little stability, yielding a dynamic on- and off-binding of monomers and larger oligomers, which has been observed for other amyloid fibril systems (Carulla et al., 2005).

In conclusion, we present the structure of recombinant α-Syn(1-121) fibrils determined at a resolution of 3.4 Å by cryo-EM. Our structure encompasses nearly the complete protein (residues 38 to 95), and includes the NAC region (residues 61 to 95) of α-Syn. We determined that various residues associated with familial forms of PD and other synucleinopathies are located in the interacting region between two protofilaments, suggesting their involvement in fibril formation and stabilization. The cryo-EM structure presented here reveals how two protofilaments interact to form a fibril, and how the NAC region contributes to protofilament formation and stability. Our structure also presents novel insights into how several PD-relevant mutations of α-Syn would compromise the structure of this fibril, suggesting that in the case of certain familial forms of PD, a different structure of α-Syn than this fibril strain might be involved. Our findings on protofilament interaction and our hypothesis on the mechanism of fibril elongation invite for the design of molecules for diagnostics or treatment of synucleinopathies.

Materials and Methods

Recombinant proteins

Recombinant full-length α-Syn was expressed from the pRT21 expression vector in BL21(DE3) competent *Escherichia coli* (*E. coli*). For N-terminal acetylation of α-Syn, cells were pre-transfected by pNatB vector coding for the N-terminal acetylase complex (plasmid kindly provided by Daniel Mulvihill, School of Biosciences, University of Kent, Canterbury, UK) (Johnson et al., 2010). C-terminally truncated forms of α-Syn(1-119), α-Syn(1-121), and α-Syn(1-122) were expressed in BL21-DE3-pLysS competent *E. coli* (plasmids courtesy of Prothena Biosciences, South San Francisco, CA, USA). Purification of α-Syn strains was performed by periplasmic lysis, ion exchange chromatography, ammonium sulfate precipitation, and gel filtration chromatography as previously described (Huang et al., 2005; Luk et al., 2009). Polo like kinase 2 (PLK2) was expressed in BL21-DE3-pLysS competent *E. coli*, isolated via its His-tag and immediately used to phosphorylate purified α-Syn. This was followed by standard ion exchange and gel filtration chromatography to separate phosphorylated from non-phosphorylated α-Syn. Endotoxins were removed from all α-Syn strains by Detoxi-Gel Endotoxin Removing Gel (Thermo Scientific) usually in one run or until endotoxin levels were below detection level. The sequence of the expressed α-Syn strains was verified by tryptic digestion followed by MALDI mass spectrometry (MS) or HPLC/ESI tandem MS for total mass was performed. Purity and monodispersity was determined by Coomassie blue or Silver staining of the SDS PAGE gel and analytical ultracentrifugation and the concentration was determined by the bicinchoninic acid (BCA) assay (Thermo Scientific) with bovine serum albumin as a standard. Dialyzed and lyophilized α-Syn(1-121) was prepared by dialyzing the purified protein in a 2 kD Slide-A-Lyzer unit (Thermo Scientific, for max. 3 ml) against HPLC-water (VWR). 500 µg protein aliquots were pipetted into 1.5ml tubes, frozen on dry ice, and lyophilized for 2h using an Eppendorf concentrator (Eppendorf). Lyophilized samples were stored at -80°C until use.

Fibrillization

Fibrils were prepared by dissolving dialyzed and lyophilized, recombinant α-Syn protein at 5 mg/mL in incubation buffer (DPBS, Gibco; 2.66mM KCL, 1.47mM KH_2PO4, 137.93mM NaCl, 8.06mM Na_2HPO_4-$7H_2O$ pH 7.0 – 7.3). Reactions of 200 µL per tube were incubated at 37°C with constant agitation (1,000 rpm) in an orbital mixer (Eppendorf). Reactions were stopped after 5 days, sonicated (5 min in a Branson 2510 water bath), aliquoted, and stored at -80°C until use. The presence of amyloid fibrils was confirmed by thioflavin T fluorimetry and high molecular weight assemblies were visualized by gel electrophoresis.

Electron microscopy

Cryo-EM grids were prepared using a Vitrobot Mark IV (ThermoFisher Scientific) with 95% humidity at 4 ºC. Amyloid fibrils (3 µL aliquots) were applied onto glow-discharged, 300 mesh, copper Quantifoil grids. After blotting, grids were plunge frozen in liquid ethane cooled by liquid nitrogen. Samples were imaged on a Titan Krios (ThermoFisher Scientific) transmission electron microscope, operated at 300 kV and equipped with a Gatan Quantum-LS imaging energy filter (GIF, 20eV energy loss window; Gatan Inc.). Images were acquired on a K2 Summit electron counting direct detection camera (Gatan Inc.) in dose fractionation mode (50 frames) using the Serial EM software (Mastronarde, 2005) at a magnification of 165,000× (physical pixel size 0.831 Å) and a total dose of ~69 electrons per square angstrom ($e^-/Å^2$) for each micrograph. Micrographs were drift-corrected and dose-weighted using MotionCor2 (Zheng et al., 2017) through the Focus interface (Biyani et al., 2017). Additional data collection parameters are detailed in Table 1.

Image processing

Helical reconstruction was carried out with the RELION 2.1 software (Scheres, 2012), using methods described in (He and Scheres, 2017). Filaments were manually selected using the helix picker in RELION 2.1. Filament segments were extracted using a box size of 280 pixels (233 Å) and an inter-box distance of 28 pixels. A total of 18,860 segments were extracted from 792 fibrils manually picked from 118 micrographs (Table 1). 2D classification was carried out with a regularization value of T=10, and 2D class averages with a clear separation of β-strands were selected for further data processing. Power spectra of 2D class averages show the layer line at 1/(4.9 Å) with peak intensities on both sides of the meridian (Bessel order n=1). This is the result of an approximate 2_1 screw symmetry between α-Syn subunits on the two protofilaments (Figure 1 – figure supplement 2). Segments assigned to the best 2D classes were used for 3D classification using a regularization value of T=8 and with optimization of the helical twist and rise. For both 3D classification and refinement, a *helical_z_percentage* parameter of 10% was used, which defines the size of the central part of the intermediate asymmetrical reconstruction that is used to apply real-space helical symmetry (He and Scheres, 2017). An initial reconstruction was calculated using a cylinder generated via the helix toolbox in RELION 2.1 as initial model. This reconstruction was low-pass filtered to 60 Å and employed as the initial model for a 3D classification with a single class (K=1) and T=20, an approach that allowed the successful reconstruction of amyloid filaments (Fitzpatrick et al., 2017).

Refinement was carried out by the auto-refine procedure with optimization of helical twist and rise. This resulted in a structure with overall resolution of 3.8 Å. Post-processing with a soft-edge mask and an estimated map sharpening *B*-factor of -82.6 Å gave a map with a resolution of 3.4 Å (by the FSC 0.143 criterion). An estimation of local resolution was obtained using RELION 2.1 and a local-resolution-filtered map was calculated for model building and refinement.

Model building and refinement

A model of the α-Syn(1-121) fibril was built into the Relion local resolution-filtered map using COOT (Emsley and Cowtan, 2004), with the PDB ID 2N0A as an initial model for the early interpretation of the map. The structure helped to determine the directionality of the protein chain and facilitated the assignment of densities in the map to specific residues. However, due to the large differences between the NMR structure and our EM map, major rebuilding was necessary. The high quality of the EM map allowed us to unambiguously build residues 38-95. A comparison was also carried out between our structure and X-ray structures of α-Syn fragments 69-77 (PDB ID 4RIK), 68-78 (PDB ID 4RIL) and 47-56 (PDB ID 4ZNN; with the mutation A53T).

The structure (10 monomers, 5 on each protofilament) was refined against the RELION local resolution-filtered map with PHENIX real space refine (Afonine et al., 2013). Rotamer, Ramachandran restraints, and "NCS" constraints were imposed, and two *B*-factors per residue were used during refinement. For validation, we randomized the coordinates (with a mean shift of 0.3 Å) and refined (using the same settings) against one of the refinement half-maps (half-map 1). We then calculated the FSC between that model (after refinement against half-map 1) and half-map 1, as well as the FSC between the same model and half-map 2 (against which it was not refined). The lack of large discrepancies between both FSC curves indicates no overfitting took place.

Competing interest statement

We note that authors D. Mona, M. E. Lauer, and M. Britschgi are employed by Hoffmann-La Roche. There are no competing interests to declare.

Data availability

The cryo-EM image data are available in the Electron Microscopy Public Image Archive, entry number EMPIAR-10195. The 3D map is available in the EMDB, entry number EMD-4276. The atomic coordinates are available at the PDB, entry number PDB 6FLT.

Acknowledgments

We thank Liz Spycher, Jana Ebner, Alexandra Kronenberger, Daniel Schlatter, Daniela Huegin, Ralph Thoma, Christian Miscenic, Martin Siegrist, Sylwia Huber, Arne Rufer, Eric Kusznir, Peter Jakob, Tom Dunkley, Joerg Hoernschmeyer, and Johannes Erny at Roche for their technical support to clone, express, purify and characterize the different recombinant forms of α-Syn, Kenneth N. Goldie, Lubomir Kovacik and Ariane Fecteau-Lefebvre for support in cryo-EM, Shirley A. Müller for support in manuscript preparation, and Sjors Scheres for help in image processing. Calculations were performed using the high-performance computing (HPC) infrastructure administered by the scientific computing center at University of Basel (sciCORE; http://scicore.unibas.ch). This work was in part supported by the Synapsis Foundation Switzerland, and the Swiss National Science Foundation (grants CRSII3_154461 and CRSII5_177195). The authors declare no competing financial interests.

References

Afonine, P.V., Headd, J.J., Terwilliger, T.C., Adams, P.D., 2013. New tool: phenix_real_space_refine. Comp. Crystal. Newsletter 4, 43-44.

Anderson, J.P., Walker, D.E., Goldstein, J.M., de Laat, R., Banducci, K., Caccavello, R.J., Barbour, R., Huang, J., Kling, K., Lee, M., Diep, L., Keim, P.S., Shen, X., Chataway, T., Schlossmacher, M.G., Seubert, P., Schenk, D., Sinha, S., Gai, W.P., Chilcote, T.J., 2006. Phosphorylation of Ser-129 is the dominant pathological modification of alpha-synuclein in familial and sporadic Lewy body disease. J. Biol. Chem. 281, 29739-29752.

Appel-Cresswell, S., Vilarino-Guell, C., Encarnacion, M., Sherman, H., Yu, I., Shah, B., Weir, D., Thompson, C., Szu-Tu, C., Trinh, J., Aasly, J.O., Rajput, A., Rajput, A.H., Jon Stoessl, A., Farrer, M.J., 2013. Alpha-synuclein p.H50Q, a novel pathogenic mutation for Parkinson's disease. Mov. Disord. 28, 811-813.

Arima, K., Ueda, K., Sunohara, N., Arakawa, K., Hirai, S., Nakamura, M., Tonozuka-Uehara, H., Kawai, M., 1998. NACP/alpha-synuclein immunoreactivity in fibrillary components of neuronal and oligodendroglial cytoplasmic inclusions in the pontine nuclei in multiple system atrophy. Acta Neuropathol 96, 439-444.

Bassil, F., Fernagut, P.-O., Bezard, E., Pruvost, A., Leste-Lasserre, T., Hoang, Q.Q., Ringe, D., Petsko, G.A., Meissner, W.G., 2016. Reducing C-terminal truncation mitigates synucleinopathy and neurodegeneration in a transgenic model of multiple system atrophy. Proc. Natl. Acad. Sci. U. S. A. 113, 9593-9598.

Biyani, N., Righetto, R.D., McLeod, R., Caujolle-Bert, D., Castano-Diez, D., Goldie, K.N., Stahlberg, H., 2017. Focus: The interface between data collection and data processing in cryo-EM. J. Struct. Biol. 198, 124-133.

Bousset, L., Pieri, L., Ruiz-Arlandis, G., Gath, J., Jensen, P.H., Habenstein, B., Madiona, K., Olieric, V., Bockmann, A., Meier, B.H., Melki, R., 2013. Structural and functional characterization of two alpha-synuclein strains. Nat. Commun. 4, 2575.

Carulla, N., Caddy, G.L., Hall, D.R., Zurdo, J., Gairi, M., Feliz, M., Giralt, E., Robinson, C.V., Dobson, C.M., 2005. Molecular recycling within amyloid fibrils. Nature 436, 554-558.

Chen, M., Margittai, M., Chen, J., Langen, R., 2007. Investigation of alpha-synuclein fibril structure by site-directed spin labeling. J. Biol. Chem. 282, 24970-24979.

Clayton, D.F., George, J.M., 1998. The synucleins: a family of proteins involved in synaptic function, plasticity, neurodegeneration and disease. Trends Neurosci. 21, 249-254.

Crowther, R.A., Daniel, S.E., Goedert, M., 2000. Characterisation of isolated alpha-synuclein filaments from substantia nigra of Parkinson's disease brain. Neurosci. Lett. 292, 128-130.

Crowther, R.A., Jakes, R., Spillantini, M.G., Goedert, M., 1998. Synthetic filaments assembled from C-terminally truncated alpha-synuclein. FEBS Lett. 436, 309-312.

Danzer, K.M., Haasen, D., Karow, A.R., Moussaud, S., Habeck, M., Giese, A., Kretzschmar, H., Hengerer, B., Kostka, M., 2007. Different species of alpha-synuclein oligomers induce calcium influx and seeding. J. Neurosci. 27, 9220-9232.

De Genst, E.J., Guilliams, T., Wellens, J., O'Day, E.M., Waudby, C.A., Meehan, S., Dumoulin, M., Hsu, S.T., Cremades, N., Verschueren, K.H., Pardon, E., Wyns, L., Steyaert, J., Christodoulou, J., Dobson, C.M., 2010. Structure and properties of a complex of alpha-synuclein and a single-domain camelid antibody. J. Mol. Biol. 402, 326-343.

Der-Sarkissian, A., Jao, C.C., Chen, J., Langen, R., 2003. Structural organization of alpha-synuclein fibrils studied by site-directed spin labeling. J. Biol. Chem. 278, 37530-37535.

Dettmer, U., Ramalingam, N., von Saucken, V.E., Kim, T.E., Newman, A.J., Terry-Kantor, E., Nuber, S., Ericsson, M., Fanning, S., Bartels, T., Lindquist, S., Levy, O.A., Selkoe, D., 2017. Loss of native alpha-synuclein multimerization by strategically mutating its amphipathic helix causes abnormal vesicle interactions in neuronal cells. Hum. Mol. Genet. 26, 3466-3481.

Dufty, B.M., Warner, L.R., Hou, S.T., Jiang, S.X., Gomez-Isla, T., Leenhouts, K.M., Oxford, J.T., Feany, M.B., Masliah, E., Rohn, T.T., 2007. Calpain-cleavage of alpha-synuclein: connecting proteolytic processing to disease-linked aggregation. Am. J. Pathol. 170, 1725-1738.

Emsley, P., Cowtan, K., 2004. Coot: model-building tools for molecular graphics. Acta Crystallogr. D Biol. Crystallogr. 60, 2126-2132.

Feany, M.B., Bender, W.W., 2000. A Drosophila model of Parkinson's disease. Nature 404, 394-398.

Fitzpatrick, A.W.P., Falcon, B., He, S., Murzin, A.G., Murshudov, G., Garringer, H.J., Crowther, R.A., Ghetti, B., Goedert, M., Scheres, S.H.W., 2017. Cryo-EM structures of tau filaments from Alzheimer's disease. Nature 547, 185-190.

Fujiwara, H., Hasegawa, M., Dohmae, N., Kawashima, A., Masliah, E., Goldberg, M.S., Shen, J., Takio, K., Iwatsubo, T., 2002. alpha-Synuclein is phosphorylated in synucleinopathy lesions. Nat. Cell. Biol. 4, 160-164.

Giasson, B.I., Murray, I.V., Trojanowski, J.Q., Lee, V.M., 2001. A hydrophobic stretch of 12 amino acid residues in the middle of alpha-synuclein is essential for filament assembly. J. Biol. Chem. 276, 2380-2386.

Gremer, L., Scholzel, D., Schenk, C., Reinartz, E., Labahn, J., Ravelli, R.B.G., Tusche, M., Lopez-Iglesias, C., Hoyer, W., Heise, H., Willbold, D., Schroder, G.F., 2017. Fibril structure of amyloid-beta(1-42) by cryo-electron microscopy. Science 358, 116-119.

Gruschus, J.M., Yap, T.L., Pistolesi, S., Maltsev, A.S., Lee, J.C., 2013. NMR structure of calmodulin complexed to an N-terminally acetylated alpha-synuclein peptide. Biochemistry (Mosc.) 52, 3436-3445.

Hasegawa, M., Fujiwara, H., Nonaka, T., Wakabayashi, K., Takahashi, H., Lee, V.M., Trojanowski, J.Q., Mann, D., Iwatsubo, T., 2002. Phosphorylated alpha-synuclein is ubiquitinated in alpha-synucleinopathy lesions. J. Biol. Chem. 277, 49071-49076.

Hashimoto, M., Rockenstein, E., Masliah, E., 2003. Transgenic models of alpha-synuclein pathology: past, present, and future. Ann. N. Y. Acad. Sci. 991, 171-188.

He, S., Scheres, S.H.W., 2017. Helical reconstruction in RELION. J. Struct. Biol. 198, 163-176.

Huang, C., Ren, G., Zhou, H., Wang, C.C., 2005. A new method for purification of recombinant human alpha-synuclein in Escherichia coli. Protein Expr. Purif. 42, 173-177.

Ibanez, P., Bonnet, A.M., Debarges, B., Lohmann, E., Tison, F., Pollak, P., Agid, Y., Durr, A., Brice, A., 2004. Causal relation between alpha-synuclein gene duplication and familial Parkinson's disease. Lancet 364, 1169-1171.

Iyer, A., Roeters, S.J., Schilderink, N., Hommersom, B., Heeren, R.M., Woutersen, S., Claessens, M.M., Subramaniam, V., 2016. The Impact of N-terminal Acetylation of alpha-Synuclein on Phospholipid Membrane Binding and Fibril Structure. J. Biol. Chem. 291, 21110-21122.

Jakes, R., Spillantini, M.G., Goedert, M., 1994. Identification of two distinct synucleins from human brain. FEBS Lett. 345, 27-32.

Johnson, M., Coulton, A.T., Geeves, M.A., Mulvihill, D.P., 2010. Targeted Amino-Terminal Acetylation of Recombinant Proteins in E. coli. PLoS ONE 5, e15801.

Kim, H.Y., Cho, M.K., Kumar, A., Maier, E., Siebenhaar, C., Becker, S., Fernandez, C.O., Lashuel, H.A., Benz, R., Lange, A., Zweckstetter, M., 2009. Structural properties of pore-forming oligomers of alpha-synuclein. J. Am. Chem. Soc. 131, 17482-17489.

Kosaka, K., Oyanagi, S., Matsushita, M., Hori, A., Iwase, S., 1976. Presenile dementia with Alzheimer-, Pick- and Lewy-body changes. Acta Neuropathol. (Berl.) 36, 221-233.

Kruger, R., Kuhn, W., Muller, T., Woitalla, D., Graeber, M., Kosel, S., Przuntek, H., Epplen, J.T., Schols, L., Riess, O., 1998. Ala30Pro mutation in the gene encoding alpha-synuclein in Parkinson's disease. Nat. Genet. 18, 106-108.

Lashuel, H.A., Petre, B.M., Wall, J., Simon, M., Nowak, R.J., Walz, T., Lansbury, P.T., Jr., 2002. Alpha-synuclein, especially the Parkinson's disease-associated mutants, forms pore-like annular and tubular protofibrils. J. Mol. Biol. 322, 1089-1102.

Lesage, S., Anheim, M., Letournel, F., Bousset, L., Honore, A., Rozas, N., Pieri, L., Madiona, K., Durr, A., Melki, R., Verny, C., Brice, A., French Parkinson's Disease Genetics Study, G., 2013. G51D alpha-synuclein mutation causes a novel parkinsonian-pyramidal syndrome. Ann. Neurol. 73, 459-471.

Li, D., Jones, E.M., Sawaya, M.R., Furukawa, H., Luo, F., Ivanova, M., Sievers, S.A., Wang, W., Yaghi, O.M., Liu, C., Eisenberg, D.S., 2014. Structure-based design of functional amyloid materials. J. Am. Chem. Soc. 136, 18044-18051.

Li, W., West, N., Colla, E., Pletnikova, O., Troncoso, J.C., Marsh, L., Dawson, T.M., Jakala, P., Hartmann, T., Price, D.L., Lee, M.K., 2005. Aggregation promoting C-terminal truncation of alpha-synuclein is a normal cellular process and is enhanced by the familial Parkinson's disease-linked mutations. Proc. Natl. Acad. Sci. U. S. A. 102, 2162-2167.

Liu, C.W., Giasson, B.I., Lewis, K.A., Lee, V.M., Demartino, G.N., Thomas, P.J., 2005. A precipitating role for truncated alpha-synuclein and the proteasome in alpha-synuclein aggregation: implications for pathogenesis of Parkinson disease. J. Biol. Chem. 280, 22670-22678.

Luhrs, T., Ritter, C., Adrian, M., Riek-Loher, D., Bohrmann, B., Dobeli, H., Schubert, D., Riek, R., 2005. 3D structure of Alzheimer's amyloid-beta(1-42) fibrils. Proc. Natl. Acad. Sci. U. S. A. 102, 17342-17347.

Luk, K.C., Song, C., O'Brien, P., Stieber, A., Branch, J.R., Brunden, K.R., Trojanowski, J.Q., Lee, V.M., 2009. Exogenous alpha-synuclein fibrils seed the formation of Lewy body-like intracellular inclusions in cultured cells. Proc. Natl. Acad. Sci. U. S. A. 106, 20051-20056.

Maltsev, A.S., Ying, J., Bax, A., 2012. Impact of N-terminal acetylation of alpha-synuclein on its random coil and lipid binding properties. Biochemistry (Mosc.) 51, 5004-5013.

Mastronarde, D.N., 2005. Automated electron microscope tomography using robust prediction of specimen movements. J. Struct. Biol. 152, 36-51.

Mbefo, M.K., Fares, M.B., Paleologou, K., Oueslati, A., Yin, G., Tenreiro, S., Pinto, M., Outeiro, T., Zweckstetter, M., Masliah, E., Lashuel, H.A., 2015. Parkinson disease mutant E46K enhances alpha-synuclein phosphorylation in mammalian cell lines, in yeast, and in vivo. J. Biol. Chem. 290, 9412-9427.

Nelson, R., Sawaya, M.R., Balbirnie, M., Madsen, A.O., Riekel, C., Grothe, R., Eisenberg, D., 2005. Structure of the cross-beta spine of amyloid-like fibrils. Nature 435, 773-778.

Oueslati, A., Fournier, M., Lashuel, H.A., 2010. Role of post-translational modifications in modulating the structure, function and toxicity of alpha-synuclein: implications for Parkinson's disease pathogenesis and therapies. Prog. Brain Res. 183, 115-145.

Oueslati, A., Paleologou, K.E., Schneider, B.L., Aebischer, P., Lashuel, H.A., 2012. Mimicking phosphorylation at serine 87 inhibits the aggregation of human alpha-synuclein and protects against its toxicity in a rat model of Parkinson's disease. J. Neurosci. 32, 1536-1544.

Outeiro, T.F., Putcha, P., Tetzlaff, J.E., Spoelgen, R., Koker, M., Carvalho, F., Hyman, B.T., McLean, P.J., 2008. Formation of toxic oligomeric alpha-synuclein species in living cells. PLoS ONE 3, e1867.

584 Paleologou, K.E., Oueslati, A., Shakked, G., Rospigliosi, C.C., Kim, H.Y., Lamberto, G.R.,
585 Fernandez, C.O., Schmid, A., Chegini, F., Gai, W.P., Chiappe, D., Moniatte, M., Schneider,
586 B.L., Aebischer, P., Eliezer, D., Zweckstetter, M., Masliah, E., Lashuel, H.A., 2010.
587 Phosphorylation at S87 is enhanced in synucleinopathies, inhibits alpha-synuclein
588 oligomerization, and influences synuclein-membrane interactions. J. Neurosci. 30, 3184-
589 3198.

590 Pasanen, P., Myllykangas, L., Siitonen, M., Raunio, A., Kaakkola, S., Lyytinen, J., Tienari, P.J.,
591 Poyhonen, M., Paetau, A., 2014. Novel alpha-synuclein mutation A53E associated with
592 atypical multiple system atrophy and Parkinson's disease-type pathology. Neurobiol. Aging
593 35, 2180 e2181-2185.

594 Peelaerts, W., Bousset, L., Van der Perren, A., Moskalyuk, A., Pulizzi, R., Giugliano, M., Van den
595 Haute, C., Melki, R., Baekelandt, V., 2015. alpha-Synuclein strains cause distinct
596 synucleinopathies after local and systemic administration. Nature 522, 340-344.

597 Periquet, M., Fulga, T., Myllykangas, L., Schlossmacher, M.G., Feany, M.B., 2007. Aggregated
598 alpha-synuclein mediates dopaminergic neurotoxicity in vivo. J. Neurosci. 27, 3338-3346.

599 Polymeropoulos, M.H., Lavedan, C., Leroy, E., Ide, S.E., Dehejia, A., Dutra, A., Pike, B., Root, H.,
600 Rubenstein, J., Boyer, R., Stenroos, E.S., Chandrasekharappa, S., Athanassiadou, A.,
601 Papapetropoulos, T., Johnson, W.G., Lazzarini, A.M., Duvoisin, R.C., Di Iorio, G., Golbe,
602 L.I., Nussbaum, R.L., 1997. Mutation in the alpha-synuclein gene identified in families with
603 Parkinson's disease. Science 276, 2045-2047.

604 Prasad, K., Beach, T.G., Hedreen, J., Richfield, E.K., 2012. Critical role of truncated alpha-synuclein
605 and aggregates in Parkinson's disease and incidental Lewy body disease. Brain Pathol. 22,
606 811-825.

607 Rao, J.N., Jao, C.C., Hegde, B.G., Langen, R., Ulmer, T.S., 2010. A combinatorial NMR and EPR
608 approach for evaluating the structural ensemble of partially folded proteins. J. Am. Chem.
609 Soc. 132, 8657-8668.

610 Reynolds, N.P., Adamcik, J., Berryman, J.T., Handschin, S., Zanjani, A.A.H., Li, W., Liu, K., Zhang,
611 A., Mezzenga, R., 2017. Competition between crystal and fibril formation in molecular
612 mutations of amyloidogenic peptides. Nat. Commun. 8, 1338.

613 Riek, R., 2017. The Three-Dimensional Structures of Amyloids. Cold Spring Harb. Perspect. Biol. 9.

614 Rodriguez, J.A., Ivanova, M.I., Sawaya, M.R., Cascio, D., Reyes, F.E., Shi, D., Sangwan, S.,
615 Guenther, E.L., Johnson, L.M., Zhang, M., Jiang, L., Arbing, M.A., Nannenga, B.L., Hattne,
616 J., Whitelegge, J., Brewster, A.S., Messerschmidt, M., Boutet, S., Sauter, N.K., Gonen, T.,
617 Eisenberg, D.S., 2015. Structure of the toxic core of alpha-synuclein from invisible crystals.
618 Nature 525, 486-490.

619 Scheres, S.H., 2012. RELION: implementation of a Bayesian approach to cryo-EM structure
620 determination. J. Struct. Biol. 180, 519-530.

621 Singleton, A.B., Farrer, M., Johnson, J., Singleton, A., Hague, S., Kachergus, J., Hulihan, M.,
622 Peuralinna, T., Dutra, A., Nussbaum, R., Lincoln, S., Crawley, A., Hanson, M., Maraganore,
623 D., Adler, C., Cookson, M.R., Muenter, M., Baptista, M., Miller, D., Blancato, J., Hardy, J.,
624 Gwinn-Hardy, K., 2003. alpha-Synuclein locus triplication causes Parkinson's disease.
625 Science 302, 841.

626 Spillantini, M.G., Crowther, R.A., Jakes, R., Hasegawa, M., Goedert, M., 1998. α-Synuclein in
627 filamentous inclusions of Lewy bodies from Parkinson’s disease and dementia with Lewy
628 bodies. Proceedings of the National Academy of Sciences 95, 6469-6473.

629 Spillantini, M.G., Schmidt, M.L., Lee, V.M., Trojanowski, J.Q., Jakes, R., Goedert, M., 1997. Alpha-
630 synuclein in Lewy bodies. Nature 388, 839-840.

631 Stefanis, L., 2012. alpha-Synuclein in Parkinson's disease. Cold Spring Harb Perspect Med 2,
632 a009399.

633 Taschenberger, G., Garrido, M., Tereshchenko, Y., Bahr, M., Zweckstetter, M., Kugler, S., 2012.
634 Aggregation of alphaSynuclein promotes progressive in vivo neurotoxicity in adult rat
635 dopaminergic neurons. Acta Neuropathol 123, 671-683.

636 Thakur, P., Breger, L.S., Lundblad, M., Wan, O.W., Mattsson, B., Luk, K.C., Lee, V.M.Y.,
637 Trojanowski, J.Q., Bjorklund, A., 2017. Modeling Parkinson's disease pathology by
638 combination of fibril seeds and alpha-synuclein overexpression in the rat brain. Proc. Natl.
639 Acad. Sci. U. S. A. 114, E8284-E8293.

640 Tu, P.H., Galvin, J.E., Baba, M., Giasson, B., Tomita, T., Leight, S., Nakajo, S., Iwatsubo, T.,
641 Trojanowski, J.Q., Lee, V.M., 1998. Glial cytoplasmic inclusions in white matter
642 oligodendrocytes of multiple system atrophy brains contain insoluble alpha-synuclein. Ann.
643 Neurol. 44, 415-422.

644 Tuttle, M.D., Comellas, G., Nieuwkoop, A.J., Covell, D.J., Berthold, D.A., Kloepper, K.D., Courtney,
645 J.M., Kim, J.K., Barclay, A.M., Kendall, A., Wan, W., Stubbs, G., Schwieters, C.D., Lee,
646 V.M., George, J.M., Rienstra, C.M., 2016. Solid-state NMR structure of a pathogenic fibril of
647 full-length human alpha-synuclein. Nat. Struct. Mol. Biol. 23, 409-415.

648 Tyson, T., Senchuk, M., Cooper, J.F., George, S., Van Raamsdonk, J.M., Brundin, P., 2017. Novel
649 animal model defines genetic contributions for neuron-to-neuron transfer of alpha-synuclein.
650 Sci Rep 7, 7506.

651 Ueda, K., Fukushima, H., Masliah, E., Xia, Y., Iwai, A., Yoshimoto, M., Otero, D.A., Kondo, J.,
652 Ihara, Y., Saitoh, T., 1993. Molecular cloning of cDNA encoding an unrecognized component
653 of amyloid in Alzheimer disease. Proc. Natl. Acad. Sci. U. S. A. 90, 11282-11286.

654 Ulmer, T.S., Bax, A., Cole, N.B., Nussbaum, R.L., 2005. Structure and dynamics of micelle-bound
655 human alpha-synuclein. J. Biol. Chem. 280, 9595-9603.

656 Vicente Miranda, H., Szego, E.M., Oliveira, L.M.A., Breda, C., Darendelioglu, E., de Oliveira, R.M.,
657 Ferreira, D.G., Gomes, M.A., Rott, R., Oliveira, M., Munari, F., Enguita, F.J., Simoes, T.,
658 Rodrigues, E.F., Heinrich, M., Martins, I.C., Zamolo, I., Riess, O., Cordeiro, C., Ponces-
659 Freire, A., Lashuel, H.A., Santos, N.C., Lopes, L.V., Xiang, W., Jovin, T.M., Penque, D.,
660 Engelender, S., Zweckstetter, M., Klucken, J., Giorgini, F., Quintas, A., Outeiro, T.F., 2017.
661 Glycation potentiates alpha-synuclein-associated neurodegeneration in synucleinopathies.
662 Brain 140, 1399-1419.

663 Vilar, M., Chou, H.T., Luhrs, T., Maji, S.K., Riek-Loher, D., Verel, R., Manning, G., Stahlberg, H.,
664 Riek, R., 2008. The fold of alpha-synuclein fibrils. Proc. Natl. Acad. Sci. U. S. A. 105, 8637-
665 8642.

666 Villar-Pique, A., Lopes da Fonseca, T., Sant'Anna, R., Szego, E.M., Fonseca-Ornelas, L., Pinho, R.,
667 Carija, A., Gerhardt, E., Masaracchia, C., Abad Gonzalez, E., Rossetti, G., Carloni, P.,
668 Fernandez, C.O., Foguel, D., Milosevic, I., Zweckstetter, M., Ventura, S., Outeiro, T.F., 2016.
669 Environmental and genetic factors support the dissociation between alpha-synuclein
670 aggregation and toxicity. Proc. Natl. Acad. Sci. U. S. A. 113, E6506-e6515.

671 Volpicelli-Daley, L.A., Luk, K.C., Lee, V.M., 2014. Addition of exogenous alpha-synuclein
672 preformed fibrils to primary neuronal cultures to seed recruitment of endogenous alpha-
673 synuclein to Lewy body and Lewy neurite-like aggregates. Nat. Protoc. 9, 2135-2146.

674 Wang, W., Nguyen, L.T.T., Burlak, C., Chegini, F., Guo, F., Chataway, T., Ju, S., Fisher, O.S.,
675 Miller, D.W., Datta, D., Wu, F., Wu, C.-X., Landeru, A., Wells, J.A., Cookson, M.R., Boxer,
676 M.B., Thomas, C.J., Gai, W.P., Ringe, D., Petsko, G.A., Hoang, Q.Q., 2016. Caspase-1
677 causes truncation and aggregation of the Parkinson's disease-associated protein α-synuclein.
678 Proc. Natl. Acad. Sci. U. S. A. 113, 9587-9592.

Wannamaker, W., Davies, R., Namchuk, M., Pollard, J., Ford, P., Ku, G., Decker, C., Charifson, P., Weber, P., Germann, U.A., Kuida, K., Randle, J.C., 2007. (S)-1-((S)-2-{[1-(4-amino-3-chloro-phenyl)-methanoyl]-amino}-3,3-dimethyl-butanoy l)-pyrrolidine-2-carboxylic acid ((2R,3S)-2-ethoxy-5-oxo-tetrahydro-furan-3-yl)-amide (VX-765), an orally available selective interleukin (IL)-converting enzyme/caspase-1 inhibitor, exhibits potent anti-inflammatory activities by inhibiting the release of IL-1beta and IL-18. J. Pharmacol. Exp. Ther. 321, 509-516.

Wasmer, C., Lange, A., Van Melckebeke, H., Siemer, A.B., Riek, R., Meier, B.H., 2008. Amyloid fibrils of the HET-s(218-289) prion form a beta solenoid with a triangular hydrophobic core. Science 319, 1523-1526.

Winner, B., Jappelli, R., Maji, S.K., Desplats, P.A., Boyer, L., Aigner, S., Hetzer, C., Loher, T., Vilar, M., Campioni, S., Tzitzilonis, C., Soragni, A., Jessberger, S., Mira, H., Consiglio, A., Pham, E., Masliah, E., Gage, F.H., Riek, R., 2011. In vivo demonstration that alpha-synuclein oligomers are toxic. Proc. Natl. Acad. Sci. U. S. A. 108, 4194-4199.

Xie, Y.Y., Zhou, C.J., Zhou, Z.R., Hong, J., Che, M.X., Fu, Q.S., Song, A.X., Lin, D.H., Hu, H.Y., 2010. Interaction with synphilin-1 promotes inclusion formation of alpha-synuclein: mechanistic insights and pathological implication. FASEB J. 24, 196-205.

Yagi-Utsumi, M., Satoh, T., Kato, K., 2015. Structural basis of redox-dependent substrate binding of protein disulfide isomerase. Sci Rep 5, 13909.

Zarranz, J.J., Alegre, J., Gomez-Esteban, J.C., Lezcano, E., Ros, R., Ampuero, I., Vidal, L., Hoenicka, J., Rodriguez, O., Atares, B., Llorens, V., Gomez Tortosa, E., del Ser, T., Munoz, D.G., de Yebenes, J.G., 2004. The new mutation, E46K, of alpha-synuclein causes Parkinson and Lewy body dementia. Ann. Neurol. 55, 164-173.

Zhao, M., Cascio, D., Sawaya, M.R., Eisenberg, D., 2011. Structures of segments of alpha-synuclein fused to maltose-binding protein suggest intermediate states during amyloid formation. Protein Sci. 20, 996-1004.

Zheng, S.Q., Palovcak, E., Armache, J.P., Verba, K.A., Cheng, Y., Agard, D.A., 2017. MotionCor2: anisotropic correction of beam-induced motion for improved cryo-electron microscopy. Nat. Methods 14, 331-332.

Figure Legends

Figure 1

Structure of α-Syn(1-121) fibril. (A) Schematic depicting the sequence of human α-Syn. The positions of the known familial mutations are indicated. β-strand regions are indicated by arrows colored from blue to red. **(B)** Cryo-EM micrograph depicting the distribution and general appearance of α-Syn fibrils. **(C)** Cryo-EM reconstruction of α-Syn(1-121) fibrils showing two protofilaments (orange and blue). **(D)** Cross-section of (C) illustrating the clear separation of the β-strands, also shown in Figure 1 – figure supplement 3A and B. (E) Cross-section of a fibril (along the axis) illustrating the arrangement of the two protofilaments (orange and blue) and fitted atomic model. Positions of the initial (L38) and final (V95) residues fitted are indicated, as well as the initial and final residue of the NAC region (E61 to V95). Arrows indicate the location of four of the five α-Syn residues where familial mutations associated with PD occur. **(F)** Distribution of β-strands in a single protofilament of the α-Syn fibril, corresponding to residues 42 to 95. Color scheme, as in (A). **(G)** As in (F) but a perpendicular view to the fibril axis illustrating height differences in some areas of a single protofilament.

Figure 1 – figure supplement 1

Negative stain TEM images of α-Syn strains. (A) Wildtype. **(B)** Ser129 Phosphorylated. **(C)** N-terminally acetylated. **(D)** C-terminally truncated (α-Syn(1-119)). **(E)** C-terminally truncated (α-Syn(1-121)). **(F)** C-terminally truncated (α-Syn(1-122)). 0.5 mg/ml fibril preparations were stained with 2% uranyl acetate. Scale bars: 100 nm.

Figure 1 – figure supplement 2

Local resolution estimation and FSC curves. (A) Cryo-EM map with local resolution estimation; the color scale indicates resolution ranging from 3.0 Å to 4.6 Å. **(B)** Fourier shell correlation curve between two independently-refined half-maps, indicating an overall resolution of 3.4 Å. **(C)** Three examples of reference-free 2D class averages from the original dataset with their respective power spectra on the right. **(D)** 2D projections and power spectra of the 3D map. **(E)** 2D projections and power spectra of the atomic model. Arrows in power spectrum panels show the layer line at 1/(4.9 Å) with peak intensities on both sides of the meridian (Bessel order n=1), resulting from an approximate 2_1 screw symmetry between adjacent α-Syn subunits.

Figure 1 – figure supplement 3

Details of atomic model and density. **(A) (B)** Clearly resolved separation of individual β-strands along the fibril. **(C)** Extra density at the interface of adjacent protofilaments between the positively charged lysines K43 and K45 and lysine K58. **(D)** Hydrophilic region surrounding a tunnel filled with an additional density**. (E)** Phosphorylation site S87 showing the location of this residue towards the outside of the fibril. **(F)** Distal loop of a protofilament indicating residues G68, A69 and G93, which may contribute to loop stability. **(G)** Arrangement of G47 and A78, which may contribute to the interaction between E46 and K80. **(H)** Interaction between H50 and E57 in the interface region of two protofilaments, which may contribute to the stability of protofilament interaction.

Figure 2

Interface region between two protofilaments of the α-Syn(1-121) fibril. (A) View along the axis of the fibril as indicated by the red rectangle on the ribbon diagram (bottom right). **(B) (C)** Side views of the fibril with orientations indicated by arrowheads in (A) and the ribbon diagram (bottom right). Panels (B) and (C) clearly illustrate the 2_1 screw symmetry that results from the staggered arrangement of subunits.

Figure 2 – figure supplement 1

Stacking of β-strands. (A)-(D) Close-up side views of the α-Syn fibril illustrating homo- and hetero-steric zippers present in the structure. Pointers in the cross-section panel (top left) indicate the points of view for panels (A) to (D).

Figure 3

Hydrophobicity of α-Syn(1-121) fibrils. (A) Top view (fibril axis) of the hydrophobic regions (brown) in a fibril where the hydrophobic pocket at the interface between two protofilaments is evident. Hydrophobicity score from hydrophilic (-4.5, blue) to hydrophobic (4.5, brown) is indicated by the color bar. Hydrophobic residues on the outer surface of the fibril are indicated. **(B)** Close-up of the region highlighted in (A) indicating the hydrophobic core composed of alanines, valines and a single isoleucine (I88). Residues forming the hydrophilic region (blue) that surrounds the hydrophobic region of the core are also visible.

Figure 4

Comparison of α-Syn(1-121) fibrils with previous α-Syn fibril structures. (A) Overlay with the solid-state NMR structure from Tuttle, *et al.*(Tuttle et al., 2016) (green). Our α-Syn structure is orange in both overlays. **(B)** Overlay with the preNAC segment obtained by micro-ED by Rodriguez, *et al.* (Rodriguez et al., 2015) (purple). The red square in (A) indicates the area of our structure shown in (B). Residue 53 is mutated (i.e., A53T) in the micro-ED structure.

Figure 5

Hydrophobic cleft at the growing end of α-Syn(1-121) fibrils. (A) Views of opposite ends of α-Syn fibrils with the two protofilaments colored orange and blue. Regions corresponding to the location of the hydrophobic cleft are shown in a lighter shade. **(B)** Residues forming the hydrophobic cleft, including V49, V52, I88, A89 provide an entry point for residues V74-V82 of an incoming α-Syn molecule (atoms shown). Area shown in panel (B) is marked in panel (A) with a square.

Video 1

Cryo-EM structure of alpha-synuclein fibril. Details of the cryo-EM reconstruction of an alpha-synuclein fibril at 3.4 Å resolution, illustrating the interaction between two protofilaments, the 4.9 Å spacing between β-strands of a single protofilament and monomer topology in the protofilament core.

Table 1

Cryo-EM structure determination and model statistics

Data Collection	
Magnification	165000 x
Pixel size (Å)	0.831
Defocus Range (μm)	-0.8 to -2.5
Voltage	300 kV
Exposure time (s per frame)	0.2
Number of frames	50
Total dose (e/Å^2)	69 to 128
Reconstruction	
Box size (pixels)	280
Inter-box distance (pixels)	28
Micrographs	118
Manually picked fibrils	792
Initial extracted segments	18860
Segments after 2D classification	18371
Segments after 3D classification	13390
Resolution after 3D refinement (Å)	3.8
Final resolution (Å)	3.42
Estimated map sharpening *B*-factor (Å^2)	-82.6
Helical rise (Å)	2.45
Helical twist (°)	-179.5
Atomic model	
Initial model used (PDB code)	2N0A
Model resolution (Å) FSC threshold	3.07/4.15 FSC=0.143/FSC=0.5
Model resolution range (Å)	116.34 - 3.07
Map sharpening *B*-factor (Å^2)	-82.6
Model composition Non-hydrogen atoms Protein residues Ligands	 3960 580 0
B-factors (Å^2) (non-hydrogen atoms) Protein Ligand	 30.28 N.A.
R.m.s. deviations Bond lengths (Å) Bond angles (°)	 0.011 1.183
Validation MolProbity score Clashscore Poor rotamers (%)	 1.20 0.12 0.00
Ramachandran plot Favored (%) Allowed (%) Disallowed (%)	 85.71 14.29 0.00

Figure 1

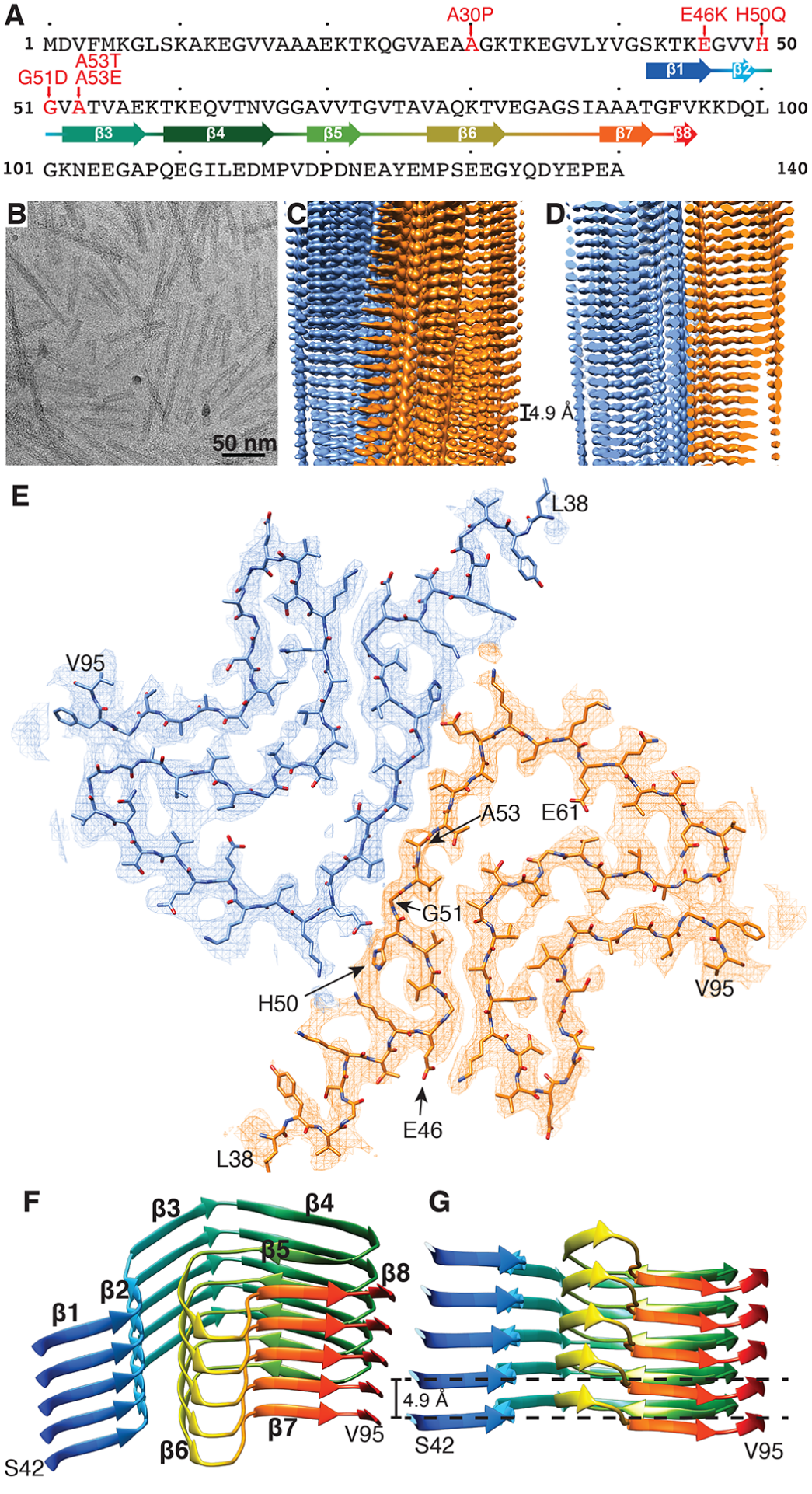
A
A30P
E46K H50Q
1 MDVFMKGLSKAKEGVVAAAEKTKQGVAEAAGKTKEGVLYVGSKTKEGVVH 50
A53T
G51D A53E
β1
β2
51 GVATVAEKTKEQVTNVGGAVVTGVTAVAQKTVEGAGSIAAATGFVKKDQL 100
β3
β4
β5
β6
β7
β8
101 GKNEEGAPQEGILEDMPVDPDNEAYEMPSEEGYQDYEPEA 140
B
50 nm
C
4.9 Å
D
E
L38
V95
A53
E61
G51
H50
V95
E46
L38
F
β3
β4
β5
β8
β2
β1
β6
β7
V95
S42
G
4.9 Å
S42
V95

Figure 1 Sup.1

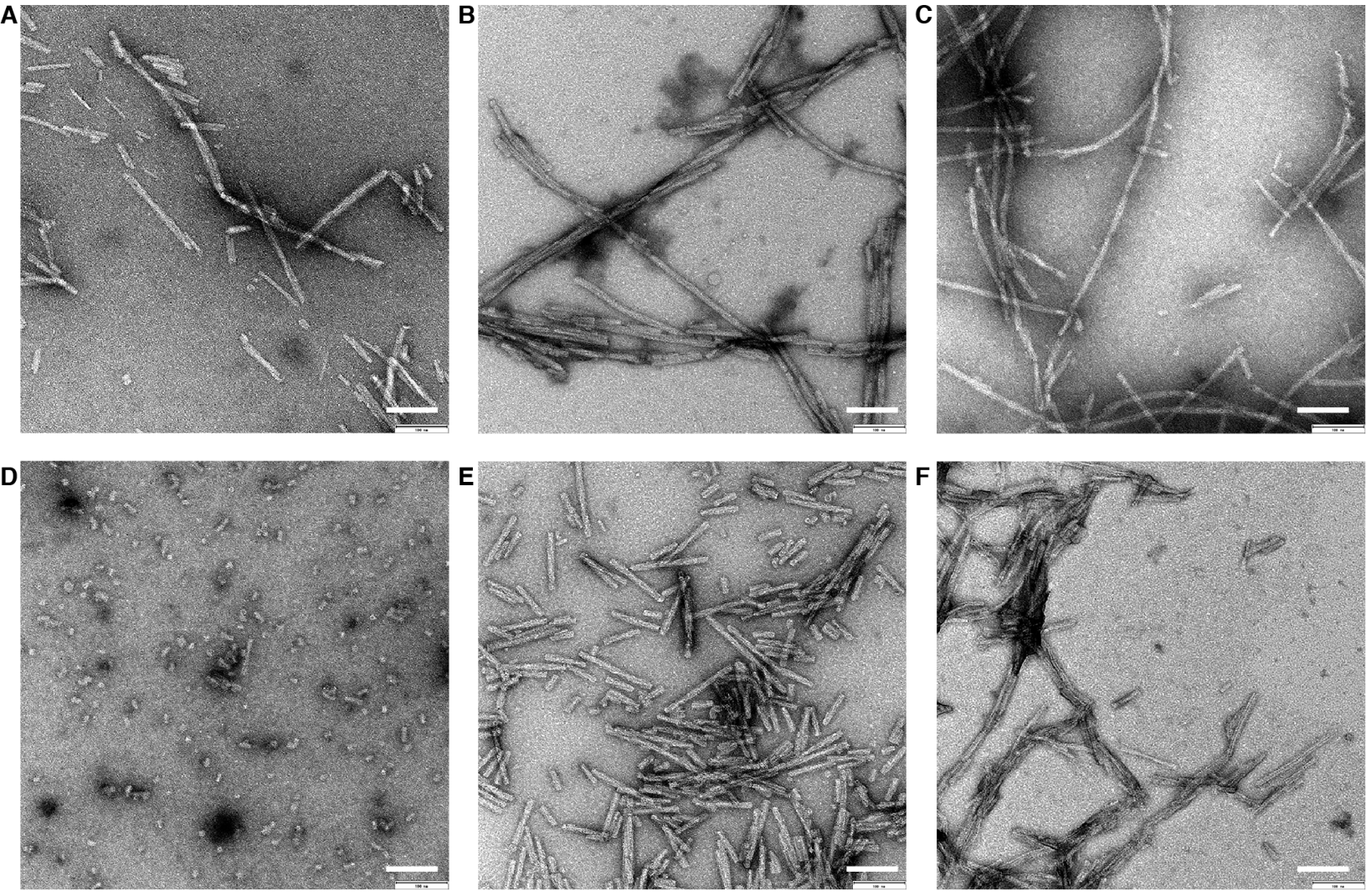

Figure 1 Sup.2

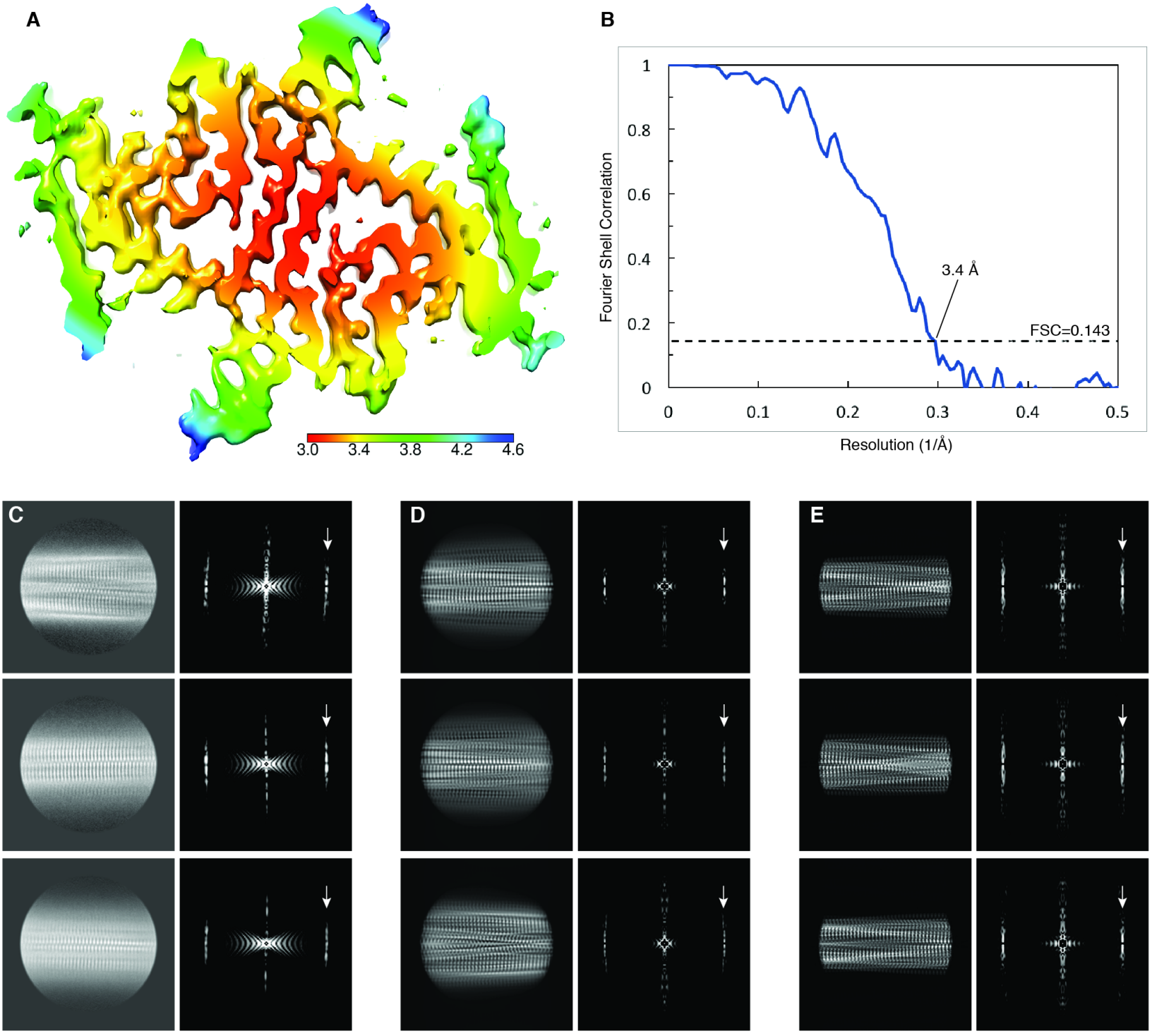

Figure 1 Sup.3

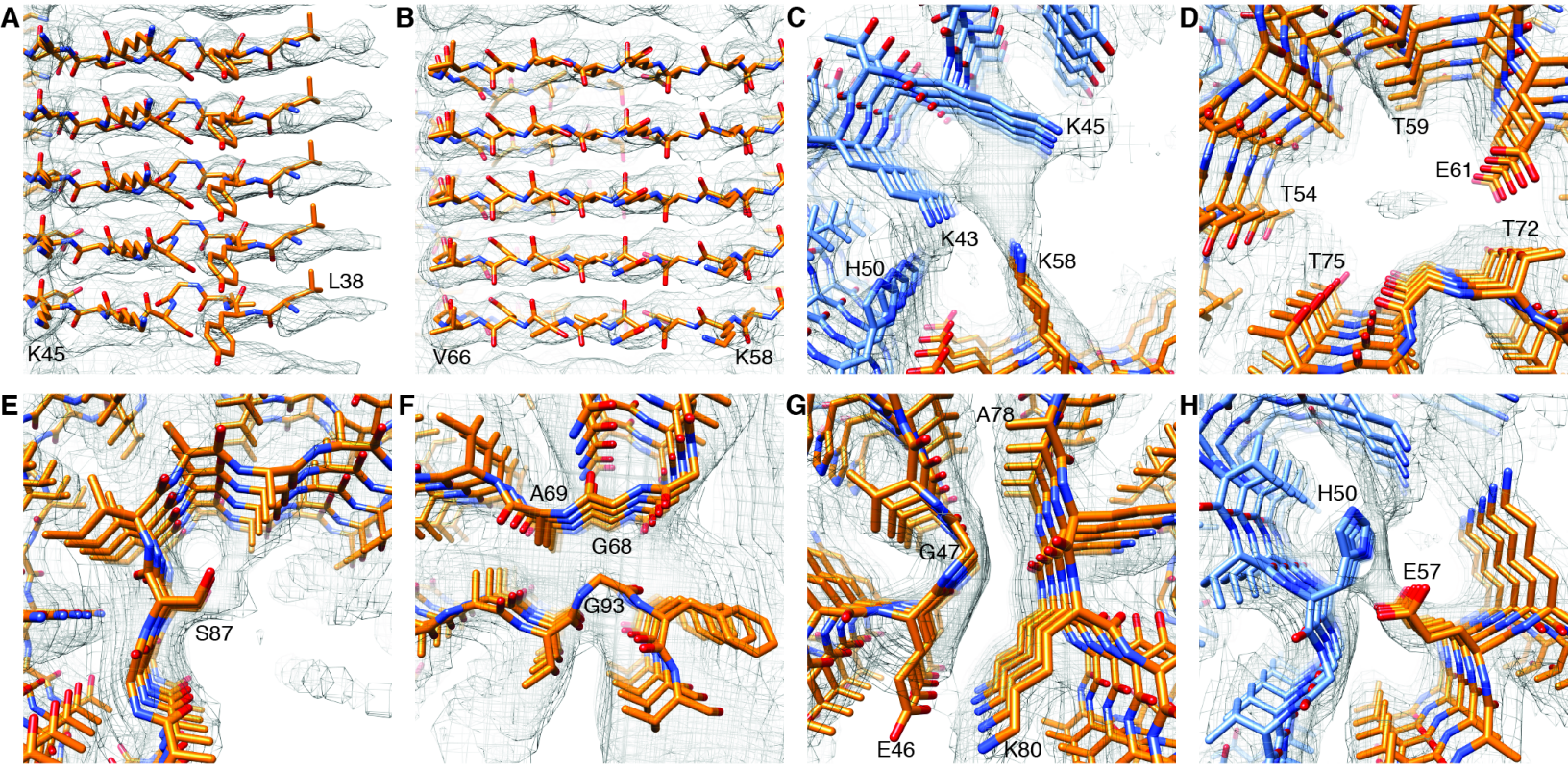

Figure 2

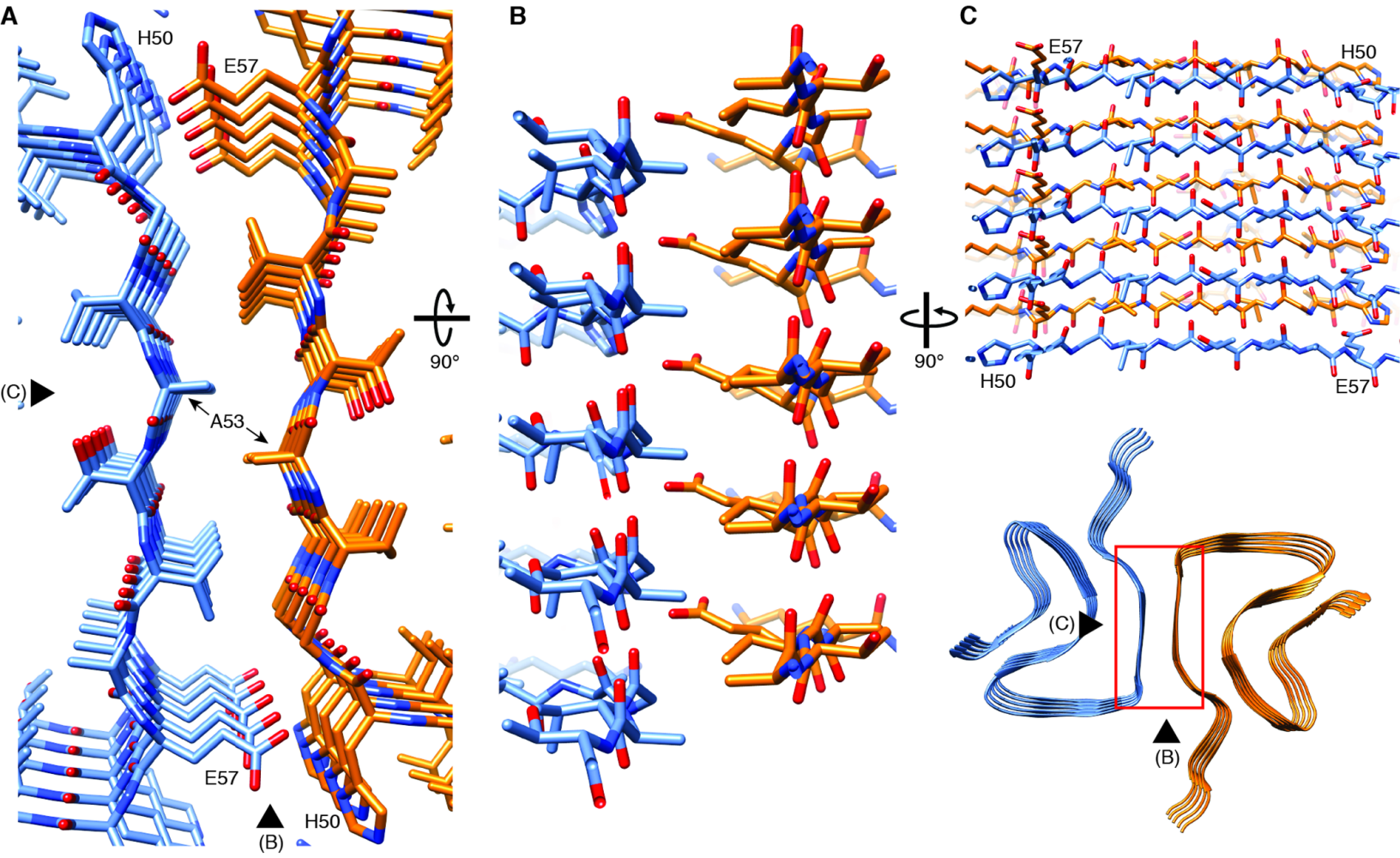

Figure 2 Sup.1

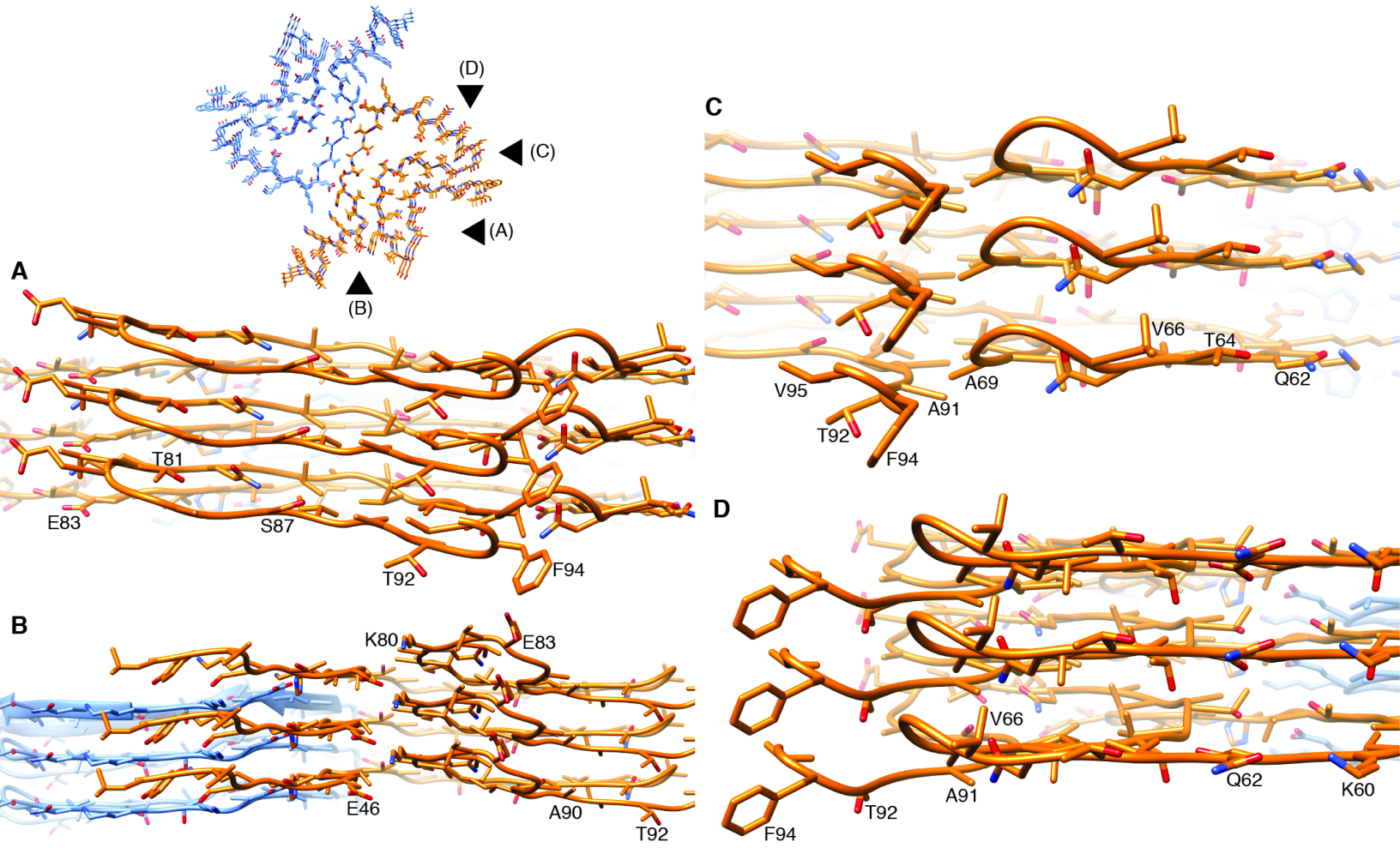

Figure 3

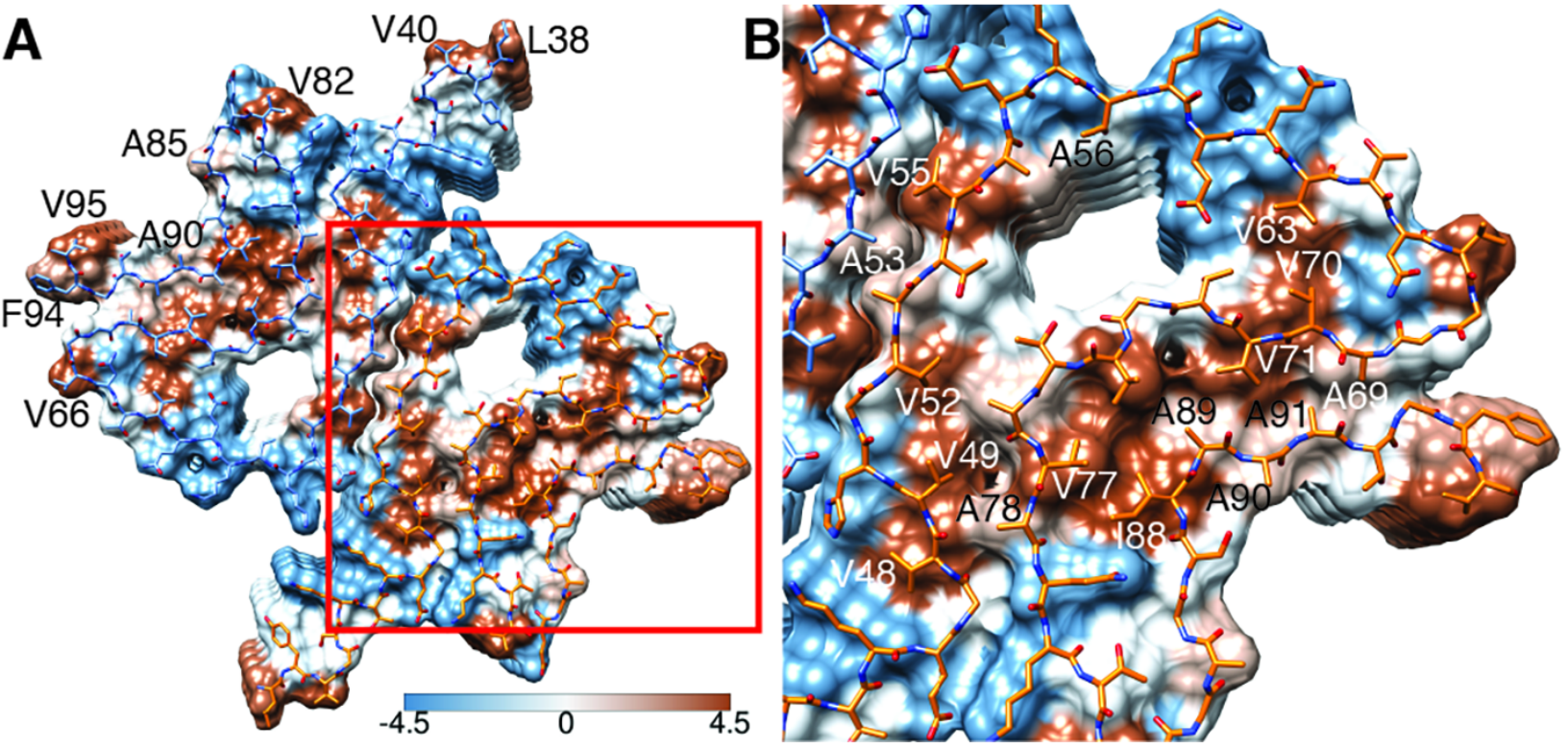
A
V40
L38
V82
A85
V95
A90
F94
V66
-4.5
0
4.5
B
V55
A56
A53
V63
V70
V71
A69
V52
A89
A91
V49
V77
A78
A90
I88
V48

Figure 4

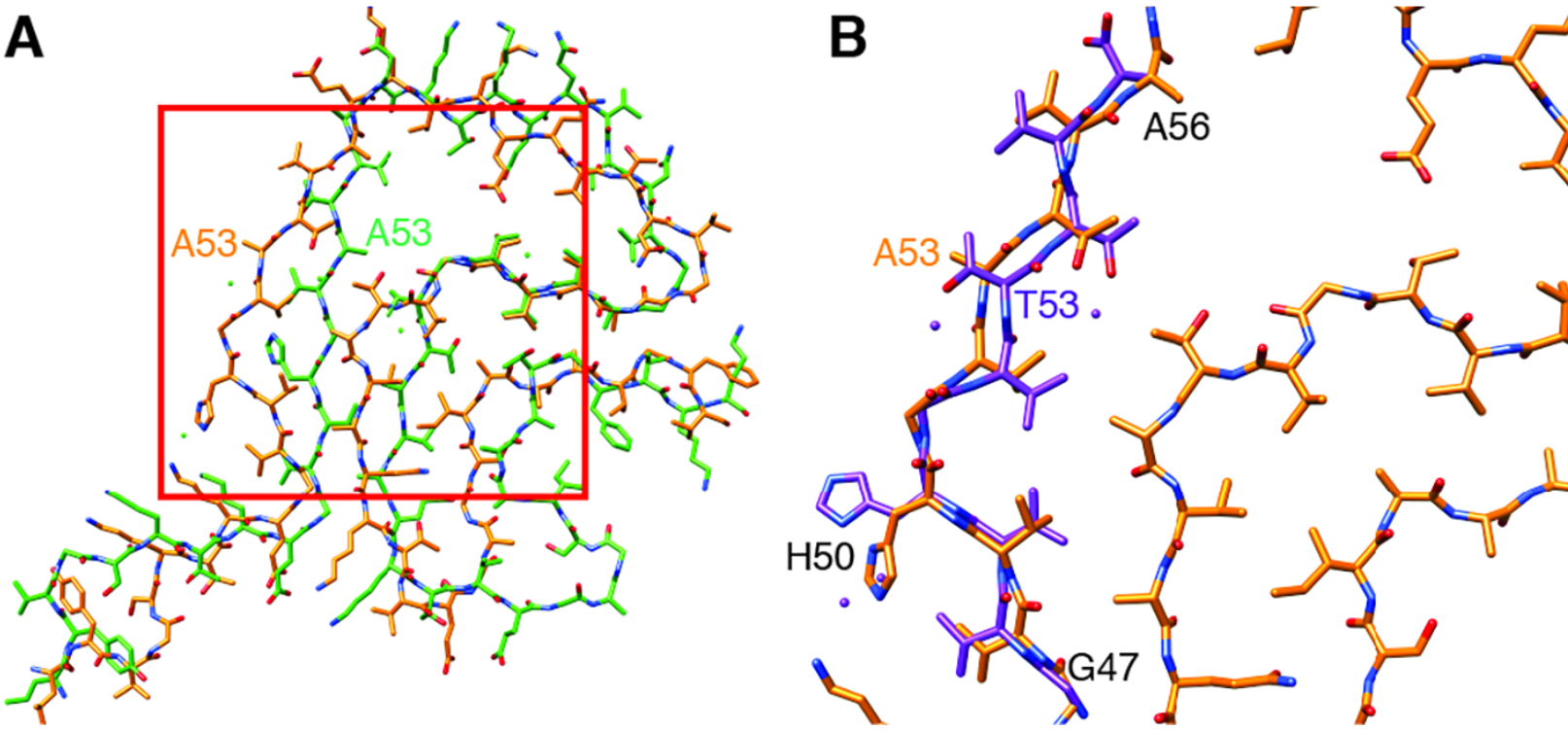

Figure 5